

Gravity-driven deformation of Damavand volcano, Iran, detected through InSAR time series

M. Shirzaei^{1*}, T.R. Walter¹, H.R. Nankali², and E.P. Holohan^{1,3}

¹Department of Physics of the Earth, Section 2.1, GFZ (GeoForschungsZentrum) Telegrafenberg, D-14473 Potsdam, Germany

²Geodesy and Geodynamics Department, National Cartographic Center, PO Box 13185-1684, Meraj Avenue, Tehran, Iran

³School of Geological Sciences, University College Dublin, Belfield, Dublin 4, Ireland

ABSTRACT

The detection and monitoring of gravity-driven volcano deformation are vital for understanding volcanic hazards such as landslides, lateral blasts, and debris avalanches. Although deformation has been detected at several large active volcanoes (e.g., Mount Etna, Vesuvius, Kilauea), these systems also exhibit persistent magmatic activity, obscuring the gravity-driven signals of ground motion. In this study we present a first interferometric synthetic aperture radar (InSAR) deformation time series at the dormant Damavand volcano in northern Iran, over the period A.D. 2003–2008. The high-resolution data show a lateral extension of the volcano at the relative rate of as much as ~6 mm/yr accompanied by subsidence at the rate of as much as ~5 mm/yr at the volcano summit. We find that lateral motion of the east flank is more significant than that of the west flank. On the basis of past understanding and modeling of deforming volcanoes elsewhere, we interpret this new evidence to reveal long-term, slow, gravity-driven deformation, possibly in the form of gravitational spreading, at Damavand. This persistent deformation activity is well expressed, although no volcanic activity was ever reported in history. This finding shows that magmatic activity is not required for spreading and highlights the importance of identifying long-lived gravity-driven deformation for hazard assessment at dormant or inactive volcanoes.

INTRODUCTION

Volcano deformation can result from the inflation or deflation of magmatic bodies, as evidenced by the very first volcano geodetic monitoring networks and utilized since in many eruption precursor studies (Dzurisin, 2006). In a geometrically simple case, ground movement associated with inflation or deflation includes uplift and outward flank motion, or subsidence and inward flank motion, respectively (Dzurisin, 2006). Other processes causing volcano deformation may involve more complex intrusion geometries, perhaps due to hydrothermal activity or perhaps entirely or partly gravity driven. The latter category includes landslides, sector collapses, and edifice spreading (flank or basal). The specific deformation pattern of those may be dissimilar from magma-driven deformation patterns; edifice spreading, for example, is often characterized by subsidence of the volcano summit, lateral extension of the upper flanks, as well as lateral contraction and uplift of the volcano's lower flanks (Borgia, 1994; van Bemmelen, 1949). Gravity-driven volcano deformation may lead to flank failure and debris avalanche generation (van Wyk de Vries and Francis, 1997); it may cause (or be caused by) coeval magmatic and volcanic activity (Froger et al., 2001; Siebert, 1992), and it may even affect subsequent magma pathways (Walter and Schmincke, 2002). Although long used to reveal deformation induced by magmatic bodies at many volcanoes around the world (Dzurisin, 2006), geodetic methods have revealed gravity-driven deformation in only a few instances (e.g., Borgia and van Wyk de Vries, 2003). Moreover, these instances have been restricted to historically active volcanoes that are generally well studied.

As this study shows, gravity-driven processes may dominate deformation at volcanoes thought to be dormant or inactive. Surface displacement

data that we have obtained by advanced interferometric synthetic aperture radar (InSAR) time series approaches reveal previously undetected but ongoing deformation at Damavand volcano in Iran. We argue that the long-term deformation field here primarily reflects a gravity-driven slow deformation process. In the following, we discuss different causes, possibly combined, that may contribute to the observed deformation pattern. These include topographic loading, buttressing and/or unbuttressing, the presence of a weak deforming volcano core, and a detachment plane underneath the volcano. Our results highlight the possibility of long-lived hazards that derive from gravity-driven deformation processes at dormant and inactive volcanoes elsewhere, and emphasize the importance of InSAR time series in their detection and volcano monitoring.

DAMAVAND TECTONIC SETTING AND VOLCANO GEOLOGY

Damavand volcano is located in the central Alborz Mountains of northern Iran (Fig. 1A), ~50 km north of Tehran, the capital city (~13 million inhabitants). The volcanic edifice is one of the largest known on land (~400 km³). It reaches an elevation of 5670 m above sea level and is the highest peak in the Middle East (Fig. 1A). Like prominent volcanoes in many other regions, Damavand also has great mythological significance as the “Persian Mount Olympus.”

The volcano is constructed upon Paleogene–Neogene tuffs, lavas, and sediments, as well as Paleozoic–Mesozoic siliciclastic, carbonate, and evaporite sequences (Allenbach, 1966). The pre-Damavand units are deformed within an east-west–trending structural grain of large folds and major thrusts and/or strike-slip faults (Figs. 2A and 2B). These faults accommodate ~5 mm/yr north-south shortening and ~4 mm/yr left lateral west-east motion (Vernant et al., 2004), and have historically generated several destructive earthquakes (Ambraseys and Melville, 1982).

Damavand is partially limited and eroded by the Haraz River, which flows south to north along the eastern side of the volcano (Fig. 1B). In this area the spatial developments of the river and volcano are thought to be intertwined; the river incises the eastern volcano flank and the adjacent topography, and the volcano's growth has locally altered the river's course (Davidson et al., 2004).

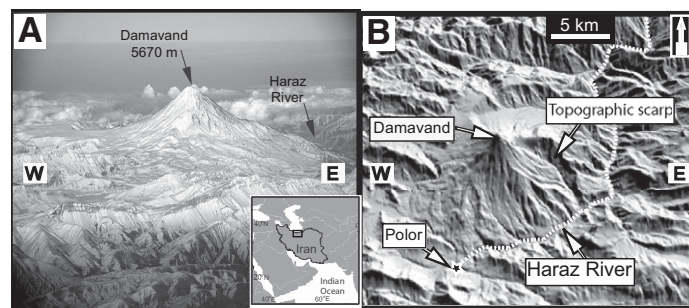


Figure 1. A: Photo of Damavand (Iran), as viewed from south, taken by Shreyans Bhansali on 10 January 2007. B: Oblique view of topography of Damavand area in northern Iran. Locations of Polor city and Haraz River are shown.

*E-mail: shirzaei@gfz-potsdam.de.

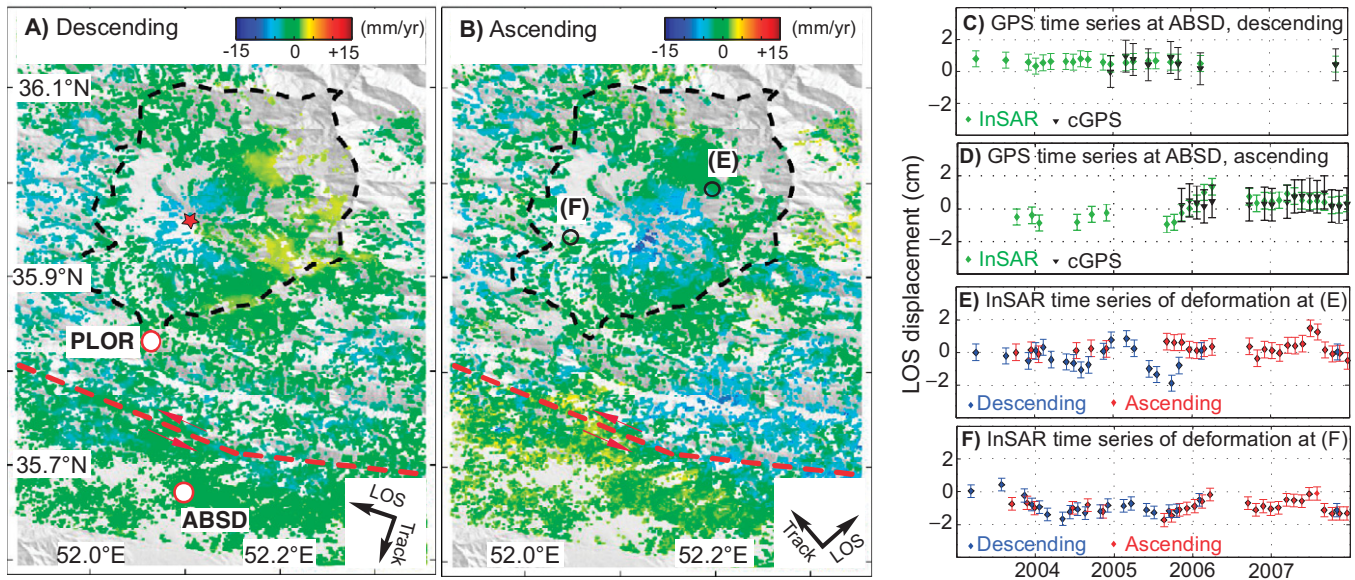


Figure 2. A: Deformation field velocity in line-of-sight (LOS) direction of satellite, as obtained in descending geometry. **B:** LOS deformation as obtained in ascending viewing geometry. Area of Damavand volcano and approximate trace of active regional tectonic faults are marked by black and red dashed lines, respectively, and locations of global positioning system (GPS) stations at Polor city (PLOR) and Absard city (ABSD) are shown. Red star—the volcano summit. **C, D:** Comparison between InSAR (interferometric synthetic aperture radar) displacement time series and GPS time series at ABSD. **E, F:** InSAR time series in descending and ascending orbit at eastern and western flank, respectively. Note that because ascending and descending data are not simultaneously acquired, LOS displacement displayed on these graphs cannot be directly compared to vertical and horizontal velocities in Figure 3.

The edifice of Damavand volcano is mainly made of trachyandesite lavas, as well as several compositionally identical fallout tuffs and at least one ignimbrite (Allenbach, 1966; Davidson et al., 2004). Geochronological and field evidence indicate two cones, constructed since at least 1.8 Ma and 0.6 Ma, respectively (Davidson et al., 2004). Although located in an area of long human habitation, no eruptive activity has been documented. The youngest preserved eruptive products are lava flows dated to ca. 7 ka. Damavand is still considered a potential volcanic hazard, as fumarolic activity persists near the summit (Davidson et al., 2004).

The volcanic history also indicates potential hazards from sector collapses, debris avalanches, and mud flows (Davidson et al., 2004). The localized, rapidly emplaced load of the volcano, in addition to potential weakening induced by ongoing hydrothermal and/or the relatively recent magmatic activity, means that Damavand may represent a more acute hazard than hillslope failures typical of such mountainous regions. Therefore, a closer evaluation of the volcano is of great importance; we next present evidence that Damavand volcano is actively deforming.

DEFORMATION FIELD AT DAMAVAND VOLCANO

To detect and characterize the deformation field at Damavand volcano, we used multiple radar images acquired by the European Space Agency satellite ENVISAT. The data set includes 20 images in descending orbit (track 106) and 25 images in ascending orbit (track 285), and spans the period A.D. 2003–2008. Using these data sets, we generated 153 and 77 interferograms in ascending and descending mode, with maximum spatial and temporal baselines of 450 m and 4 yr, respectively (for examples, see the GSA Data Repository¹). To obtain unambiguous phase changes, we unwrapped the modulo 2π phase observations of each interferogram using a two-dimensional (2-D) minimum cost flow algorithm

¹GSA Data Repository item 2011091, examples of generated interferograms in ascending and descending satellite orbit track, is available online at www.geosociety.org/pubs/ft2011.htm, or on request from editing@geosociety.org or Documents Secretary, GSA, P.O. Box 9140, Boulder, CO 80301, USA.

(Chen and Zebker, 2001; Costantini, 1998). Phase unwrapping is applied only to those pixels exhibiting a low decorrelation noise (Costantini and Rosen, 1999). The algorithm for identifying low-noise pixels was derived from earlier works (Berardino et al., 2002; Ferretti et al., 2001; Hooper et al., 2007). The differential phase changes of the interferograms were inverted (Bjerhammar, 1973) to generate a time series of the displacement in the line of sight (LOS) represented at each pixel (Schmidt and Bürgmann, 2003). The filter for reducing the atmospheric phase screen is derived following Ferretti et al. (2001) and was applied by using a time frequency analysis (Daubechies, 1992).

Figures 2A and 2B show maps of the linear velocity field as seen in LOS for both the descending and ascending orbit. The precisions of the displacement time series and the linear velocity field are estimated using the standard variance-covariance matrices of the differential phase inversion and of the robust regression (Mikhail, 1976; O’Leary, 1990). The variance-covariance matrices provide us with 2 mm and 0.5 mm/yr precision for the displacement time series and the linear velocity field, respectively. In the vicinity of Damavand summit to the east, a slight displacement increase of +2 mm/yr is detected in the descending viewing geometry (Fig. 2A), whereas a displacement decrease of as much as –12 mm/yr is seen in ascending viewing geometry (Fig. 2B).

To validate the results of the InSAR time series and to estimate their accuracy, we compared them against independent data sets. In the study area there are two continuous global positioning system (cGPS) stations equipped with Ashtech receivers and choke ring antennas (PLOR and ABSD in Fig. 2A). These two high-quality stations are part of Iranian permanent GPS network, which is maintained by the Iranian National Cartographic Center. The cGPS signal is sampled every 30 s. Daily observations are jointly adjusted with the observations of surrounding International Global Navigation Satellite System (GNSS) service (IGS) stations using the GAMIT processing routine (King and Bock, 2002) and IGS precise orbits. GLOBK is used to combine daily solutions and generate time series of the deformation field by using a Kalman Filter approach (Hofmann-Wellenhof et al., 2000). We considered the PLOR station, located outside

the Damavand volcano edifice, to be the reference station. Upon projecting the cGPS data to the LOS viewing geometry, the InSAR and cGPS data show very good agreement (Figs. 2C and 2D). The error bars are estimated in the 95% confidence region by using the maximum diagonal component of the variance-covariance matrices for both cGPS and InSAR data. This validation test allows us to reliably explore the time series of a deformation field of ~100,000 InSAR pixels. Moreover, Figures 2E and 2F present the InSAR time series of cumulative displacement in descending and ascending orbit mode at two points on the eastern and western volcano flanks. The displacement here shows some episodic short-term fluctuation, which is accounted for in the linear regression used to calculate the long-term velocity. Investigating the cause of the short-term signals is beyond the scope of this study and will be addressed in future works. The apparent disagreement between ascending and descending displacement in Figure 2E, and the good agreement in Figure 2F, suggest lateral movement on the eastern flank and dominant vertical motion on the western flank.

The different viewing geometries of the radar satellites enabled us to constrain the west-east and vertical components of motion at Damavand volcano (Figs. 3A and 3B). Because the satellite orbits are near-polar, only a small fraction of north-south component is measured. As its LOS projected component is <0.5 mm/yr, the north-south regional-tectonic shortening across the Alborz (Vernant et al., 2004) is below the method's precision, and is thus considered to have a negligible contribution to the calculation of the east-west and vertical components. The regional tectonic strain has therefore not affected the observed local volcano deformation pattern, as described in the following.

In general, the west-east component shows a pattern characterized by extension of the volcanic edifice respect to a line trending roughly NNE–SSW (Fig. 3A). The eastern flank moves eastward at an average velocity of 5 mm/yr, while the western flank moves westward at an average velocity of <0.5 mm/yr. These values are obtained by averaging the velocity field over the entire area of each flank. However, a closer view reveals that this pattern is not uniform. On the eastern flank of the volcano, for example, the area immediately south of a prominent topographic scarp (Fig. 1B) has a locally higher eastward velocity of as much as 10 mm/yr (A in Fig. 3A). This area could represent a faster moving sector. Another heterogeneity to the general pattern, marked B in Figure 3A, shows a gradient in the velocity field. This may be an area subject to slow local-

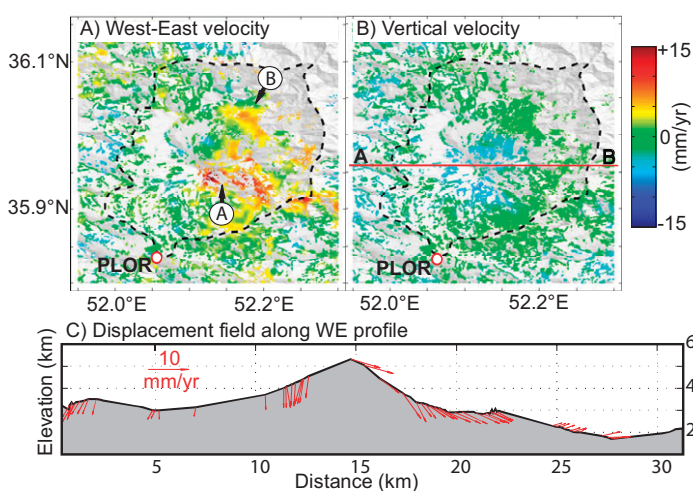


Figure 3. A: West-east velocity field. Area of rapid eastward motion is marked by letter A; letter B denotes anomalies to general trend in displacement field. PLOR—Polar city global positioning system station. B: Vertical velocity field. C: West-east (WE) profile of observed deformation field with respect to volcano topography. This profile highlights that volcano is slowly spreading eastward.

ized fault reactivation. The vertical component (Fig. 3B) shows a radially symmetric deformation pattern characterized by an average subsidence of ~5 mm/yr at the summit. On the eastern flank the subsidence quickly declines to zero near the volcano base.

To better visualize the deformation field with respect to the volcano morphology, a west-east cross section is shown in Figure 3C. The displacement vectors at the profile surface are those measured from our InSAR data set. The western side of the profile shows a predominant subsidence and a slight westward component of motion. The eastern side shows a more heterogeneous deformation profile, and a main feature is the stronger component of horizontal motion (toward the east). At km 22–25 in Figure 3C, at the base of the eastern flank, the sense of deformation changes from subsidence to uplift.

DISCUSSION

From an advanced InSAR deformation time series, we have observed subsidence at Damavand volcano that decreases from the volcano summit area toward the flanks. Subsidence is accompanied by outward-directed lateral motions that are more pronounced on the eastern flank.

The observed surface displacements are not directly compatible with any simple inflation or deflation of a magmatic body (Dzurisin, 2006). For example, a vertically elongated inflating reservoir (Yang et al., 1988) may generate summit subsidence but also a broad uplift of the flanks; the latter was not found at Damavand. Overall, the most promising mechanism explaining surface displacements patterns at Damavand volcano is gravity-driven spreading (Figs. 3A and 3B). Spreading may be induced by a weak substratum or a weak volcano core (Cecchi et al., 2005; Delcamp et al., 2008). Surface displacement fields associated with volcano spreading have been isolated and quantified foremost in laboratory-based analogue models. Although there may be some degree of freedom concerning the direction and amplitude of deformation (Borgia et al., 2000; Wooller et al., 2004), the displacement patterns for model volcano spreading are characterized by summit subsidence, outward-directed lateral movement of the flanks, and basal uplift, as observed at Damavand (Figs. 3A and 3B).

The asymmetry of deformation at Damavand that we interpret as a more pronounced spreading toward the east may result from numerous factors. These include a dipping substratum (Wooller et al., 2004), the direction of regional slope (Francis and Wells, 1988), buttressing or unbuttressing (Borgia et al., 1992), or lateral inhomogeneities in the edifice or in its basement (Cecchi et al., 2005). At Damavand, high topography at the west may lead to lateral displacement to the east, whereas erosion caused by the Haraz River incising downward at ~1 km/m.y. (Davidson et al., 2004) may create the space necessary for lateral spreading to the east (cf. Fig. 1B). The gentler slope of the eastern flank compared to the western flank is also compatible with greater spreading of the eastern with respect to the western flank (van Wyk de Vries and Borgia, 1996).

Such asymmetry is not unusual. For example, at Mount Etna volcano, Sicily (Borgia et al., 1992), a combination of dipping weak substrata, regional slope, and buttressing/unbuttressing of the edifice has led to more pronounced spreading on its eastern flank. Moreover, as at Damavand, deformation at Mount Etna is heterogeneous with structural sectors that move at different velocities (Froger et al., 2001). A key difference is that Mount Etna is magmatically active while Damavand is not, which highlights that magmatic forcing is not required for spreading, as reported in earlier studies (Borgia and van Wyk de Vries, 2003; van Bemmelen, 1949).

Structures typically associated with an unstable volcano flank include normal faults on the upper flank, a main décollement underneath the flank, and thrusts and/or strike-slip faults on the lowermost flank (Borgia and van Wyk de Vries, 2003; Merle and Borgia, 1996). The presence of such structures or those accounting for deformation heterogeneities is as yet unconstrained at Damavand volcano, which has not been studied in detail and requires close field inspection.

Gravity-driven volcano deformation may lead to sector collapses and debris avalanches, and direct the locations of coeval or later eruptions (Lipman and Mullineaux, 1981; Siebert, 1992; Walter and Amelung, 2006). At Damavand volcano, there is evidence for at least one large sector collapse that dammed the regional drainage (Davidson et al., 2004). In addition to affecting local population centers and those downstream along the Haraz River, the recurrence of such an event could pose major problems for populations (e.g., Tehran city) that are highly dependent on the Damavand water sources. Future extension of the time series may help to forecast a collapse event if ground motions showed acceleration.

SUMMARY AND CONCLUSION

We have used InSAR time series to detect and characterize a deformation field for the first time at the dormant Damavand volcano in northern Iran. We observed subsidence of the summit and predominantly eastward-directed spreading of the flanks. Gravity-driven spreading is the most likely explanation of these long-term observations. Several factors, possibly combined, may facilitate this, including a dipping weak substratum, a weak volcano core, topographic buttressing in the west, and erosional unbuttressing in the east. Our results illustrate the potential for long-lived hazard from gravity-driven processes at dormant or inactive volcanoes and the importance of geodetic techniques in their detection and monitoring.

ACKNOWLEDGMENTS

We thank three anonymous reviewers and Roland Burgmann for helpful comments and discussions. Shirzaei acknowledges funding through the Geotechnological Program "Managing Volcano Unrest." Walter acknowledges a grant from the Emmy-Noether fellowship (WA1642-1/4). Holohan acknowledges an INSPIRE postdoctoral fellowship cofunded by Marie Curie Actions and the Irish Research Council for Science, Engineering and Technology.

REFERENCES CITED

Allenbach, P., 1966, Geologie und petrographie des Damavand und seiner umgeurg (Zentral-Elburz), Iran: Geologisches Institut, ETH-Zurich, Mitteilung Nr. 63, 114 p.

Ambraseys, N.N., and Melville, C.P., 1982, A history of Persian earthquakes: London, Cambridge University Press, 219 p.

Berardino, P., Fornaro, G., Lanari, R., and Sansosti, E., 2002, A new algorithm for surface deformation monitoring based on small baseline differential SAR interferograms: IEEE Transactions on Geoscience and Remote Sensing, v. 40, p. 2375–2383, doi: 10.1109/TGRS.2002.803792.

Bjerhammar, A., 1973, Theory of errors and generalized matrix inverse: Amsterdam, Elsevier, p. 127–128.

Borgia, A., 1994, Dynamic basis of volcanic spreading: Journal of Geophysical Research, v. 99, p. 17,791–17,804, doi: 10.1029/94JB00578.

Borgia, A., Ferrari, L., and Pasquare, G., 1992, Importance of gravitational spreading in the tectonic and volcanic evolution of Mount Etna: Nature, v. 357, p. 231–235, doi: 10.1038/357231a0.

Borgia, A., Delaney, P.T., and Denlinger, R.P., 2000, Spreading volcanoes: Annual Review of Earth and Planetary Sciences, v. 28, p. 539–570.

Borgia, A., and van Wyk de Vries, B., 2003, The volcano-tectonic evolution of Concepcion, Nicaragua: Bulletin of Volcanology, v. 65, p. 248–266, doi: 10.1007/s00445-002-0256-8.

Cecchi, E., Van Wyk de Vries, B., and Lavest, J.M., 2005, Flank spreading and collapse of weak-cored volcanoes: Bulletin of Volcanology, v. 67, p. 72–91, doi: 10.1007/s00445-004-0369-3.

Chen, C.W., and Zebker, H.A., 2001, Two-dimensional phase unwrapping with use of statistical models for cost functions in nonlinear optimization: Optical Society of America Journal, v. 18, p. 338–351, doi: 10.1364/JO-SAA.18.000338.

Costantini, M., 1998, A novel phase unwrapping method based on network programming: IEEE Transactions on Geoscience and Remote Sensing, v. 36, p. 813–821, doi: 10.1109/36.673674.

Costantini, M., and Rosen, P.A., 1999, A generalized phase unwrapping approach for sparse data: Proceedings of the IEEE 1999 International Geoscience and Remote Sensing Symposium (IGARSS), Volume 1, p. 267–269, doi: 10.1109/IGARSS.1999.773467.

Daubechies, I., 1992, Ten lectures on wavelets: Philadelphia, Pennsylvania, Society for Industrial and Applied Mathematics, 377 p.

Davidson, J., Hassanzadeh, J., Berzin, R., Stockli, D.F., Bashukooh, B., Turrin, B., and Pandamouz, A., 2004, The geology of Damavand volcano, Alborz

Mountains, northern Iran: Geological Society of America Bulletin, v. 116, p. 16–29, doi: 10.1130/B25344.1.

Delcamp, A., van Wyk de Vries, B., and James, M.R., 2008, The influence of edifice slope and substrata on volcano spreading: Journal of Volcanology and Geothermal Research, v. 177, p. 925–943, doi: 10.1016/j.jvolgeores.2008.07.014.

Dzurisin, D., 2006, Volcano deformation—New geodetic monitoring techniques: Berlin, Springer-Verlag, 476 p.

Ferretti, A., Prati, C., and Rocca, F., 2001, Permanent scatterers in SAR interferometry: IEEE Transactions on Geoscience and Remote Sensing, v. 39, p. 8–20, doi: 10.1109/36.898661.

Francis, P.W., and Wells, G.L., 1988, Landsat Thematic Mapper observations of debris avalanche deposits in the Central Andes: Bulletin of Volcanology, v. 50, p. 258–278, doi: 10.1007/BF01047488.

Froger, J.-L., Merle, O., and Briole, P., 2001, Active spreading and regional extension at Mount Etna imaged by SAR interferometry: Earth and Planetary Science Letters, v. 187, p. 245–258, doi: 10.1016/S0012-821X(01)00290-4.

Hofmann-Wellenhof, B., Lichtenegger, H., and Collins, J., 2000, Global positioning system, theory and practice (fifth edition): New York, Springer, 390 p.

Hooper, A., Segall, P., and Zebker, H., 2007, Persistent scatterer interferometric synthetic aperture radar for crustal deformation analysis, with application to Volcán Alcedo, Galápagos: Journal of Geophysical Research, v. 112, p. 1–21, doi: 10.1029/2006JB004763.

King, R.W., and Bock, Y., 2002, Documentation for the GAMIT GPS analysis software: Cambridge, Massachusetts Institute of Technology, and San Diego, California, Scripps Institution of Oceanography, 206 p.

Lipman, P.W., and Mullineaux, D.R., eds., 1981, The 1980 eruptions of Mount St. Helens: U.S. Geological Survey Professional Paper 1250, 844 p.

Merle, O., and Borgia, A., 1996, Scaled experiments of volcano spreading: Journal of Geophysical Research, v. 101, p. 13,805–13,817, doi: 10.1029/95JB03736.

Mikhail, E.M., 1976, Observations and least squares: New York, IEP Publishers, 497 p.

O’Leary, D.P., 1990, Robust regression computation using iteratively reweighted least square: SIAM Journal on Matrix Analysis and Applications, v. 11, p. 466–480, doi: 10.1137/0611032.

Schmidt, D.A., and Bürgmann, R., 2003, Time-dependent land uplift and subsidence in the Santa Clara valley, California, from a large interferometric synthetic aperture radar data set: Journal of Geophysical Research, v. 108, p. 1–13, doi: 10.1029/2002JB002267.

Siebert, L., 1992, Threats from debris avalanches: Nature, v. 356, p. 658–659, doi: 10.1038/356658a0.

van Bemmelen, R.W., 1949, The geology of Indonesia: The Hague, Government Printing Office, 732 p.

van Wyk de Vries, B., and Borgia, A., 1996, The role of basement in volcano deformation, in McQuire, W.J., et al., eds., Volcano instability on the Earth and other planets: Geological Society of London Special Publication 110, p. 95–110, doi: 10.1144/GSL.SP.1996.110.01.07.

van Wyk de Vries, B., and Francis, P., 1997, Catastrophic collapse at stratovolcanoes induced by gradual volcano spreading: Nature, v. 387, p. 387–390, doi: 10.1038/387387a0.

Vernant, P., Nilforoushan, F., Chery, J., Bayer, R., Djamour, Y., Masson, F., Nankali, H., Ritz, J.F., Sedighi, M., and Tavakoli, F., 2004, Deciphering oblique shortening of central Alborz in Iran using geodetic data: Earth and Planetary Science Letters, v. 223, p. 177–185, doi: 10.1016/j.epsl.2004.04.017.

Walter, T.R., and Amelung, F., 2006, Volcano-earthquake interaction at Mauna Loa volcano, Hawaii: Journal of Geophysical Research, v. 111, no. B5, doi: 10.1029/2005JB003861.

Walter, T.R., and Schmincke, H.-U., 2002, Rifting, recurrent landsliding and Miocene structural reorganization on NW-Tenerife (Canary Islands): International Journal of Earth Sciences, v. 91, p. 615–628, doi: 10.1007/s00531-001-0245-8.

Wooller, L., van Wyk de Vries, B., Murray, J.B., Rymer, H., and Meyer, S., 2004, Volcano spreading controlled by dipping substrata: Geology, v. 32, p. 573–576, doi: 10.1130/G20472.1.

Yang, X.M., Davis, P.M., and Dieterich, J.H., 1988, Deformation from inflation of a dipping finite prolate spheroid in an elastic half space as a model for volcanic stressing: Journal of Geophysical Research, v. 93, p. 4249–4257, doi: 10.1029/JB093iB05p04249.

Manuscript received 23 September 2010

Revised manuscript received 6 October 2010

Manuscript accepted 8 October 2010

Printed in USA